Atomic layer deposition of Zn(O,S) thin films with tunable electrical properties by oxygen annealing

Atomic Layer Deposition of Zn(O,S) Thin Films with Tunable Electrical Properties by Oxygen Annealing

Helen Hejin Park, Rachel Heasley, and Roy G. Gordon[a)]

School of Engineering and Applied Sciences, Department of Chemistry and Chemical Biology, Harvard University, Cambridge, Massachusetts, USA

Abstract

Zinc oxysulfide, Zn(O,S), films grown by atomic layer deposition (ALD) were annealed in oxygen to adjust the carrier concentration. The electron carrier concentration of Zn(O,S) can be reduced by several orders of magnitude from 10^{19} to 10^{15} cm^{-3} by post-deposition annealing in oxygen at temperatures from 200°C to 290°C. In the case of Zn(O,S) with S/Zn = 0.37, despite the considerable change in the electron carrier concentration, the bandgap energy decreased by only ~0.1 eV, and the crystallinity did not change much after annealing. The oxygen/zinc ratio increased by 0.05 after annealing, but the stoichiometry remained uniform throughout the film.

Keywords: Zinc Oxysulfide, Buffer Layer, Atomic Layer Deposition, Thin-Film Solar Cells

[a)] Electronic mail : gordon@chemistry.harvard.edu

$Cu(In,Ga)(S,Se)_2$ (CIGS) is one of the most reliable materials used in thin-film solar cells, but currently, the most efficient CIGS-based solar cells use CdS,[1,2] a toxic material, as an *n*-type buffer layer between the *p*-type CIGS absorber layer and the ZnO/transparent conducting oxide (TCO) layers. Buffer layers are critical in reducing interface recombination and giving optimum band alignment across the junction.[3,4] It is therefore of interest to study alternative materials that better satisfy the earth-abundance and non-toxicity requirements for low-cost and environmentally compatible large-scale production. Previous research has shown that zinc oxysulfide—Zn(O,S)—grown by atomic layer deposition (ALD) is a promising alternative to CdS in CIGS solar cells.[5,6] The larger bandgap of Zn(O,S) ($E_g \approx 2.6 - 3.8$ eV) compared to the bandgap of CdS ($E_g \approx 2.4$ eV) reduces photocurrent loss in the short-wavelength region.[7] In addition, the bandgap of Zn(O,S) and the conduction band offset at the buffer/absorber interface can be finely tuned by altering the stoichiometry of Zn(O,S).[5,6,8,9] Various growth methods have been previously reported for Zn(O,S), such as sputtering,[8,10,11] chemical bath deposition (CBD),[12] pulse laser deposition (PLD),[13,14] and ALD.[5,6,15,16] ALD has the advantage of easily controlling the stoichiometry of multicomponent films by simply tailoring the pulse ratio of the precursors.

In addition to the progress of replacing CdS with Zn(O,S) buffer layers in CIGS-based solar cells, much research has also been motivated to replace the expensive indium-based CIGS absorber layer with more earth-abundant materials, such as $Cu_2ZnSn(Se,S)_4$[17-19] and SnS.[20-22] These new absorber layers need an *n*-type material partner such as Zn(O,S) to serve as a buffer layer. In fact, Zn(O,S) buffer layers have already been integrated with SnS absorber layers to produce solar cells with record efficiency for SnS-based solar cells.[23] With increasing interest in such research areas, it is important to have a better understanding of ALD Zn(O,S) and the tunability of its properties to further improve the performance of thin-film solar cells using earth-abundant and non-toxic elements.

The tunability of the electrical properties of Zn(O,S) is important since the *n*-type buffer layer will affect the recombination of free carriers at the absorber/buffer interface.[24] An optimum of carrier concentration for Zn(O,S) is needed since the carrier concentration will also affect the

Fermi energy level, which will affect the conduction-band offset as well. Studies have shown that a positive conduction-band offset ($E_{c,buffer} > E_{c,absorber}$) that is higher than ~0.4 eV will block photo-generated electrons to flow towards the TCO, whereas a negative conduction-band offset ($E_{c,buffer} < E_{c,absorber}$) will increase the recombination via defects at the buffer/absorber interface.[25] To improve solar cell device performances, recombination at the absorber/buffer interface can be reduced by decreasing the defects and tuning the conduction-band offset through the control of Zn(O,S). However, further studies on the impact of the carrier concentration of the buffer layer on the solar cell device performance are still needed. Previously, it has been shown that post-deposition annealing in oxygen can help to reduce oxygen defects, such as oxygen vacancies.[26] Oxygen vacancies contribute to the high carrier concentration in various oxides.[27] In this paper, we report that Zn(O,S) can be annealed in oxygen to reduce its electron carrier concentration by up to four orders of magnitude, with negligible influence on the bandgap and crystallinity of the potential buffer layer material.

A custom-built hot-wall ALD reactor was used to grow Zn(O,S) films approximately 100 nm thick. The precursors used were diethylzinc (DEZ, $Zn(C_2H_5)_2$, Strem Chemicals), deionized H_2O, and a gas mixture of 4% H_2S in N_2 for the zinc, oxygen, and sulfur sources, respectively. All of the precursors were kept at room temperature. The exposures used for each dose of DEZ, H_2O, and H_2S are estimated to be approximately 0.13, 0.15, and 6.50 Torr·s, respectively. Purified N_2 was used as the purging gas. The ALD sequence was $(DEZ/N_2/H_2O/N_2) \times m + (DEZ/N_2/H_2S/N_2) \times n$: for different sulfur incorporation into the films, the precursor pulse ratios were varied by tailoring m and n, reflected by the notation Zn(O,S) m:n throughout this paper. Films were grown at a deposition temperature of 120°C, and were annealed in O_2 with a constant vapor pressure of ~5.60 Torr for 1.5 hours at temperatures ranging from 200°C – 290°C.

The carrier concentration and carrier type were determined by van der Pauw measurements of the Hall effect. The carrier mobility was then evaluated from $\rho = 1/ne\mu$, where ρ is the resistivity, n is the carrier concentration, e is the electron charge, and μ is the carrier mobility. Stoichiometry of the films was measured by Rutherford backscattering spectroscopy (RBS). The optical bandgap (E_g) and absorption coefficient (α) were determined by measuring the optical transmittance and reflectance spectra[28] from a UV/visible spectrophotometer with an integrating sphere (Hitachi U-4100). The crystal structure, grain size, and texture of the films were analyzed by x-ray diffraction (XRD, PANalytical X-Pert Pro) with Cu $K\alpha$ radiation using θ-2θ scan. Cross-sectional (with 12° tilt) and plan-view morphology of films were examined by field-emission scanning electron microscopy (FESEM, Zeiss, Ultra-55). Depth profile of Zn(O,S) 7:1 oxygen annealed at 290°C was obtained by x-ray photoelectron spectroscopy (XPS, Thermo Scientific, K-Alpha). Zn(O,S) films were grown on quartz substrates for Hall, bandgap measurements, and XRD analysis, on glassy carbon substrates for RBS, and on Si(100) substrates for XPS, FESEM, and XRD.

It is reasonable to ask whether oxygen annealing increased the amount of oxygen in the films or reduced the sulfur content, either near the surface of the films or throughout the films. Rutherford backscattering spectroscopy (RBS) showed that the O/Zn ratio increased by 0.05 after oxygen annealing while the S/Zn ratio remained almost the same. Depth profiling by XPS was used to estimate the elemental distribution of O, S, Zn, Si, and C throughout the film. Figure 1 shows a uniform distribution of elements in Zn(O,S) with S/Zn = 0.37 annealed at the highest temperature (290°C). RBS also indicated uniform stoichiometry throughout the film after oxygen annealing. These results imply that the diffusion of oxygen took place throughout the film and was not confined to the surface, which is also reflected in the Hall data of Fig. 2.

The dependence of oxygen anneal temperature on the electrical properties of Zn(O,S) is shown as a function of the ratio of the sulfur content S/Zn for different oxygen anneal temperatures in Fig. 2. For the as-deposited films, Zn(O,S) 19:1, 9:1, 7:1, 6:1, 5:1, and 4:1 have S/Zn ratios of 0.09, 0.26, 0.37, 0.50, 0.64, and 0.73, respectively, and O/Zn ratios of 0.99, 0.82, 0.72, 0.64, 0.50, and 0.42, respectively, as determined by RBS analysis. Hall measurements were over the detection limit for films with high sulfur content such as Zn(O,S) with S/Zn = 0.50, 0.64, and 0.73 due to their high resistivities. Overall, the resistivity had a tendency to increase with sulfur content for the as-deposited and oxygen annealed films (Fig. 2a). For the as-deposited Zn(O,S) films, the electron carrier concentration remained around the 10^{19} cm^{-3} range despite the increase of sulfur content

(Fig. 2b). Annealing the Zn(O,S) films in O_2 decreased the carrier concentrations, with larger decreases for films with higher sulfur content. A fairly narrow anneal temperature range of 200°C to 290°C caused electron carrier concentrations in Zn(O,S) to decrease by 1 to 4 orders of magnitude. The decreases in electron carrier concentration are probably due to removal of donor defects such as oxygen vacancies.[27]

Electron carrier mobility showed a tendency to decrease with increasing sulfur content for the as-deposited films, which may be due to increased scattering from the disorder introduced by random substitution of sulfur for oxygen. However, it was difficult to notice clear trends with sulfur content in the mobility of annealed films. The mobilities of the oxygen annealed films (0.8 – 7.6 $cm^2/V \cdot s$) tended to be lower than the as-deposited films (27.5 – 27.8 $cm^2/V \cdot s$), for the films with lower sulfur content (Fig. 2c). Hall measurements of mobility were not possible for the highly resistive Zn(O,S) films with S/Zn = 0.37 annealed at 290°C.

Stability of the Zn(O,S) films was investigated by repeating the Hall measurements of films that were kept under atmosphere condition for approximately one year, as shown in Fig. 2. Carrier concentrations increased by approximately an order of magnitude after ~1 yr under atmosphere condition for films with lower carrier concentrations. This may be due to the increased hydroxyl groups within the film over time, since ZnO-based films are known for easily picking up moisture from the atmosphere.[29] The increase in carrier concentration over time was much less significant for films with higher carrier concentrations. There is no clear trend for the mobilities of the films.

Figure 3(a) shows a plot of α^2 vs. photon energy for the as-deposited ZnO and Zn(O,S) with S/Zn = 0.37, and Zn(O,S) with S/Zn = 0.37 annealed in O_2 at temperatures between 200°C and 290°C. Bandgap energy was then estimated using Tauc's relation for direct transitions:[30]

$$\alpha(h\nu) \propto (h\nu - E_g)^{1/2} \quad (1)$$

where $\alpha(h\nu)$ is the absorption coefficient, $h\nu$ is the photon energy, and E_g is the optical bandgap, assuming that the electron and hole effective masses are constant. In Fig. 3(a), the steeper slope for the as-deposited ZnO compared to the Zn(O,S) films with S/Zn = 0.37 can be qualitatively explained by the disorder-induced band-tail states of Zn(O,S). For Zn(O,S) films with S/Zn = 0.37, the bandgap energy decreased by ~0.1 eV after the film was annealed in O_2 at 200°C, but higher annealing temperatures did not have any significant additional effect on the bandgap energy, as shown in Fig. 3(b).

X-ray diffraction of the as-deposited ZnO and Zn(O,S) with S/Zn = 0.37, and Zn(O,S) with S/Zn = 0.37 annealed in O_2 at different temperatures grown on quartz substrates are shown in Fig. 4. For the as-deposited films, once sulfur was added, the films remained polycrystalline, but the peak intensities decreased. This reduction may be due to an amorphous component of the Zn(O,S) films, which does not contribute to the diffraction peaks.

The lattice constant, vertical grain size, and nonuniform distribution of local strain in the films were determined from diffraction. To separate the $K\alpha_1$ and $K\alpha_2$ peaks, double-peak Lorentzian functions were used, and the instrumental peak broadening was taken into account.[31-33] Nonuniform distribution of local strain and grain size were then estimated from the Scherrer equation of Δk vs. k (scattering vector $k = (4\pi/\lambda)\sin\theta$):[31]

$$\Delta k = \frac{\Delta d}{d} k + \frac{2\pi}{D} \quad (2)$$

where Δk is the full width at half maximum (FWHM), $\Delta d/d$ is the nonuniform distribution of local strain, and D is the grain size. Substitution of sulfur increases the lattice constant of Zn(O,S) (a = 0.336 nm) over that of ZnO (a = 0.323 nm), while Vegard's law predicts a = 0.374 nm. Oxygen annealing does not alter the lattice constant of Zn(O,S) significantly (Fig. 5a). No significant difference in grain size was found between ZnO and Zn(O,S) (Fig. 5b). This result is not consistent with previous studies that observed grain size reduction for intermediate compositions of Zn(O,S).[5,6] Although the oxygen anneal temperature had a large effect on the electrical properties of Zn(O,S) with S/Zn = 0.37, the anneal temperature did not produce any noticeable modification of the grain size and local strain, as shown in Figs. 5b and 5c. XRD analysis of Zn(O,S) films grown on quartz substrates show very similar grain size and texture to films grown on Si, as shown in Figs. S1 and S2 (see Ref. 34), which implies that the crystallization behavior of the films is independent of the substrate type.

The low dependence of oxygen anneal temperature on the vertical and lateral grain sizes

was confirmed by the cross-sectional and plan-view FESEM images shown in Fig. 6. Although the addition of sulfur to ZnO changed the shape and size of the lateral grains, it was difficult to observe any noteworthy change in the vertical and lateral grains of Zn(O,S) with S/Zn = 0.37 by oxygen annealing.

In conclusion, it was demonstrated that an anneal temperature range of only 200°C – 290°C reduced the electron carrier concentration of ALD Zn(O,S) by four orders of magnitude from 10^{19} to 10^{15} cm^{-3}. The electrical properties of Zn(O,S) are strongly affected by the sulfur content and the oxygen annealing temperature. Bandgaps of the Zn(O,S) films with S/Zn = 0.37 were shown to change by only ~0.1 eV with O_2 annealing. Although electrical properties were modified to a large extent by oxygen annealing, the annealing temperature investigated in this study had an insignificant effect on the bandgap and crystallinity of Zn(O,S) films with S/Zn = 0.37. RBS showed that oxygen was added to the films by annealing, but the sulfur content remained unchanged. Depth profiling by XPS showed that the distribution of elements through the film remained uniform after annealing in oxygen.

The authors thank Dr. Harish Bhandari and Dr. Zhefeng Li for assistance in modifying the ALD reactor, and Dr. Mark Winkler and Meng-Ju Sher for help with Hall measurements. This work was supported by the U. S. National Science Foundation (NSF, CBET-1032955) and the U.S. Department of Energy (DE-EE0005329). Part of the work was performed at the Center of Nanoscale Systems (CNS) at Harvard University, a member of the National Nanotechnology Infrastructure Network (NNIN), which is supported by NSF (ECS-0335765).

References

[1] K. Ramanathan, M. A. Contreras, C. L. Perkins, S. Asher, F. S. Hasoon, J. Keane, D. Young, M. Romero, W. Metzger, R. Noufi, J. Ward, and A. Duda, *Prog. Photovolt: Res. Appl.* **11**, 225 (2003).

[2] I. Repins, M. A. Contreras, B. Egaas, C. DeHart, J. Scharf, C. L. Perkins, B. To, and R. Noufi, *Prog. Photovolt: Res. Appl.* **16**, 235 (2008).

[3] J. Poortmans and V. Arkhipov, *Thin Film Solar Cells: Fabrication, Characterization and Applications* (Wiley, Chichester, England; Hoboken, NJ, 2007).

[4] Y. Kim, W. Lee, D. R. Jung, J. Kim, S. Nam, H. Kim, and B. Park, *Appl. Phys. Lett.* **96**, 171902 (2010).

[5] A. Hultqvist, C. Platzer-Björkman, E. Coronel, and M. Edoff, *Sol. Energy Mater. Sol. Cells* **95**, 497 (2011).

[6] C. Platzer-Björkman, T. Törndahl, D. Abou-Ras, J. Malmström, J. Kessler, and L. Stolt, *J. Appl. Phys.* **100**, 044506 (2006).

[7] S. Siebentritt, *Sol. Energy* **77**, 767 (2004).

[8] T. Minemoto, A. Okamoto, and H. Takakura, *Thin Solid Films* **519**, 7568 (2011).

[9] C. Y. Moon, S. H. Wei, Y. Z. Zhu, and G. D. Chen, *Phys. Rev. B* **74**, 233202 (2006).

[10] B. K. Meyer, A. Polity, B. Farangis, Y. He, D. Hasselkamp, T. Krämer, and C. Wang, *Appl. Phys. Lett.* **85**, 4929 (2004).

[11] A. Okamoto, T. Minemoto, and H. Takakura, *Jpn. J. Appl. Phys.* **50**, 04DP10 (2011).

[12] I. Lauermann, T. Kropp, D. Vottier, A. Ennaoui, W. Eberhardt, and E. F. Aziz, *Chemphyschem* **10**, 532 (2009).

[13] Y. Z. Yoo, Z. W. Jin, T. Chikyow, T. Fukumura, M. Kawasaki, and H. Koinuma, *Appl. Phys. Lett.* **81**, 3798 (2002).

[14] S. H. Deulkar, J. L. Huang, and M. Neumann-Spallart, *J. Electron. Mater.* **39**, 589 (2010).

[15] J. R. Bakke, J. T. Tanskanen, C. Hägglund, T. A. Pakkanen, and S. F. Bent, *J. Vac. Sci. Technol. A* **30**, 01A135 (2012).

[16] B. W. Sanders and A. Kitai, *Chem. Mater.* **4**, 1005 (1992).

[17] B. Shin, O. Gunawan, Y. Zhu, N. A. Bojarczuk, S. J. Chey, and S. Guha, *Prog. Photovoltaics* **21**, 72 (2013).

[18] H. Katagiri, K. Jimbo, S. Yamada, T. Kamimura, W. S. Maw, T. Fukano, T. Ito, and T. Motohiro, *Appl. Phys. Express* **1**, 041201 (2008).

[19] H. Katagiri, K. Saitoh, T. Washio, H. Shinohara, T. Kurumadani, and S. Miyajima, *Sol.*

H. Katagiri, K. Saito, T. Washio, H. Shinohara, T. Kurumadani, and S. Miyajima, *Sol. Energy Mater. Sol. Cells* **65**, 141 (2001).
[20] K. Hartman, J. L. Johnson, M. I. Bertoni, D. Recht, M. J. Aziz, M. A. Scarpulla, T. Buonassisi, *Thin Solid Films* **519**, 7421 (2011).
[21] K. T. Ramakrishna Reddy, N. Koteswara Reddy, and R. W. Miles, *Sol. Energy Mater. Sol. Cells* **90**, 3041 (2006).
[22] M. Sugiyama, K. Miyauchi, T. Minemura, and H. Nakanishi, *Jpn. J. Appl. Phys.* **47**, 8723 (2008).
[23] P. Sinsermsuksakul, K. Hartman, S. B. Kim, J. Heo, L. Sun, H. H. Park, R.Chakraborty, T. Buonassisi, and R. G. Gordon, *Appl. Phys. Lett.* **102**, 053901 (2013).
[24] S. Merdes, R. Sáez-Araoz, A. Ennaoui, J. Klaer, M. C. Lux-Steiner, and R. Klenk, *Appl. Phys. Lett.* **95**, 213502 (2009).
[25] T. Minemoto, T. Matsui, H. Takakura, Y. Hamakawa, T. Negami, Y. Hashimoto, T. Uenoyama, and M. Kitagawa, *Sol. Energy Mater. Sol. Cells* **67**, 83 (2001).
[26] Y. Liu, S. Shen, L. J. Brillson, and R. G. Gordon, *Appl. Phys. Lett.* **98**, 122907 (2011).
[27] M. D. McCluskey and S. J. Jokela, *J. Appl. Phys.* **106**, 071101 (2009).
[28] J. I. Pankove, *Optical Processes in Semiconductors* (Prentice-Hall, Englewood Cliffs, NJ, 1971).
[29] G. Kresse, O. Dulub, and U. Diebold, *Phys. Rev. B* **68**, 245409 (2003).
[30] J. Tauc, *Mater. Res. Bull.* **5**, 721 (1970).
[31] B. E. Warren, *X-Ray Diffraction* (Dover Publications, NY, 1990).
[32] T. Kim, J. Oh, B. Park, and K. S. Hong, *Appl. Phys. Lett.* **76**, 3043 (2000).
[33] Y. Kim, J. Oh, T. G. Kim, and B. Park, *Appl. Phys. Lett.* **78**, 2363 (2001).
[34] See supplementary figures (S1 and S2).

Figure Captions

Fig. 1. Depth profile of Zn(O,S) with S/Zn = 0.37, up to the Si substrate.

Fig. 2. Plots of (a) resistivity, (b) electron carrier concentration, and (c) electron mobility vs. S/Zn, for the as-deposited Zn(O,S) and Zn(O,S) samples annealed at 200°C, 230°C, 260°C, and 290°C in O_2. Measurements were repeated for films after ~1 yr with S/Zn = 0.37, as shown on the right side of the plots.

Fig. 3. Plots of (a) α^2 vs. $h\nu$ and (b) bandgap energy vs. O_2 annealing temperature for Zn(O,S) with S/Zn = 0.37.

Fig. 4. X-ray diffraction for the as-deposited ZnO, as-deposited Zn(O,S) with S/Zn = 0.37, and Zn(O,S) with S/Zn = 0.37, annealed in O_2 at various temperatures on quartz substrates.

Fig. 5. Plots of (a) lattice constant, (b) grain size, and (c) local strain vs. O_2 annealing temperature for the as-deposited ZnO, as-deposited Zn(O,S) with S/Zn = 0.37, and Zn(O,S) with S/Zn = 0.37, oxygen annealed at different temperatures on quartz substrates.

Fig. 6. Cross-sectional and plan-view FESEM images for the as-deposited ZnO, as-deposited Zn(O,S) with S/Zn = 0.37, and Zn(O,S) with S/Zn = 0.37, oxygen annealed at 200°C, 230°C, 260°C, and 290°C.

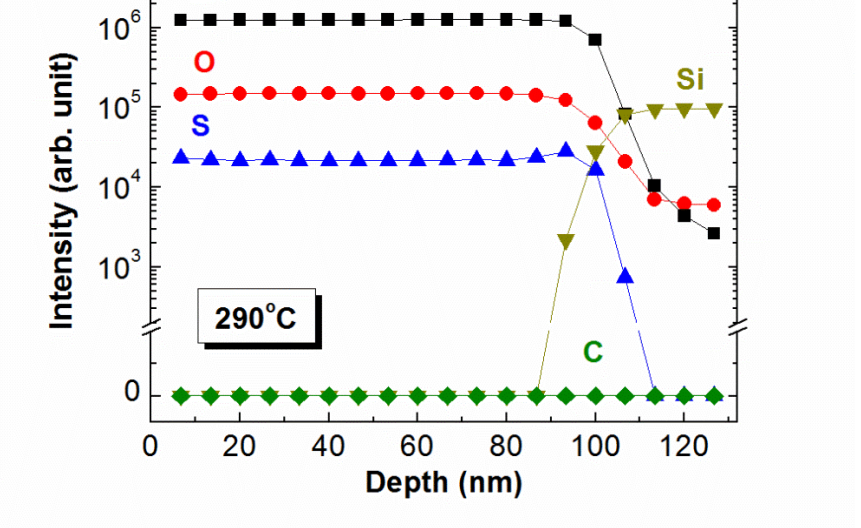

Fig. 1. Depth profile of Zn(O,S) with S/Zn = 0.37, up to the Si substrate.

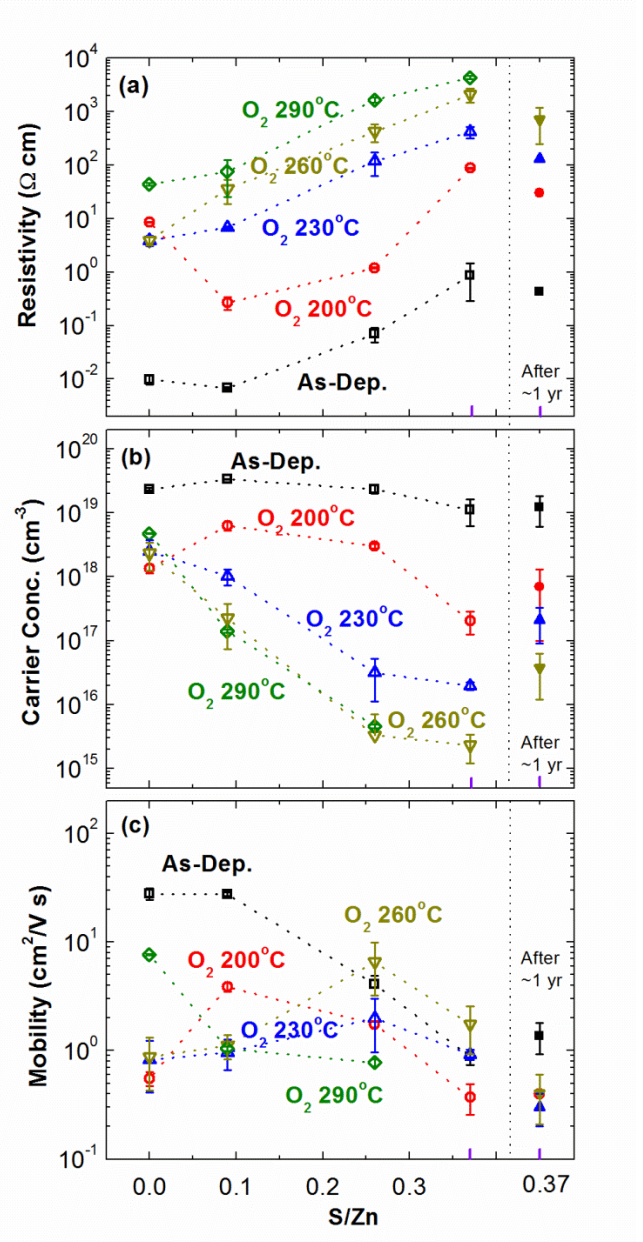

Fig. 2. Plots of (a) resistivity, (b) electron carrier concentration, and (c) electron mobility vs. S/Zn,

for the as-deposited Zn(O,S) and Zn(O,S) samples annealed at 200°C, 230°C, 260°C, and 290°C in O_2. Measurements were repeated for films after ~1 yr with S/Zn = 0.37, as shown on the right side of the plots.

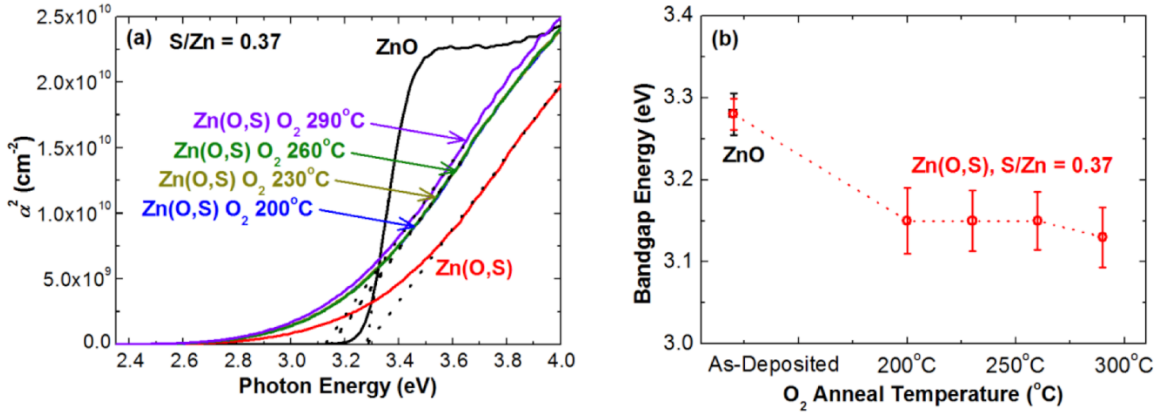

Fig. 3. Plots of (a) α^2 vs. $h\nu$ and (b) bandgap energy vs. O_2 annealing temperature for Zn(O,S) with S/Zn = 0.37.

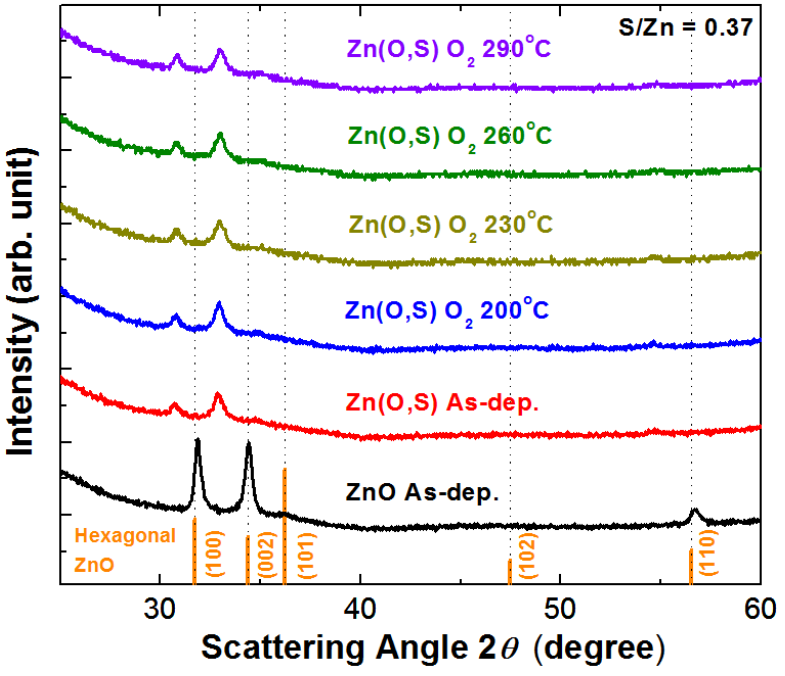

Fig. 4. X-ray diffraction for the as-deposited ZnO, as-deposited Zn(O,S) with S/Zn = 0.37, and Zn(O,S) with S/Zn = 0.37, annealed in O_2 at various temperatures on quartz substrates.

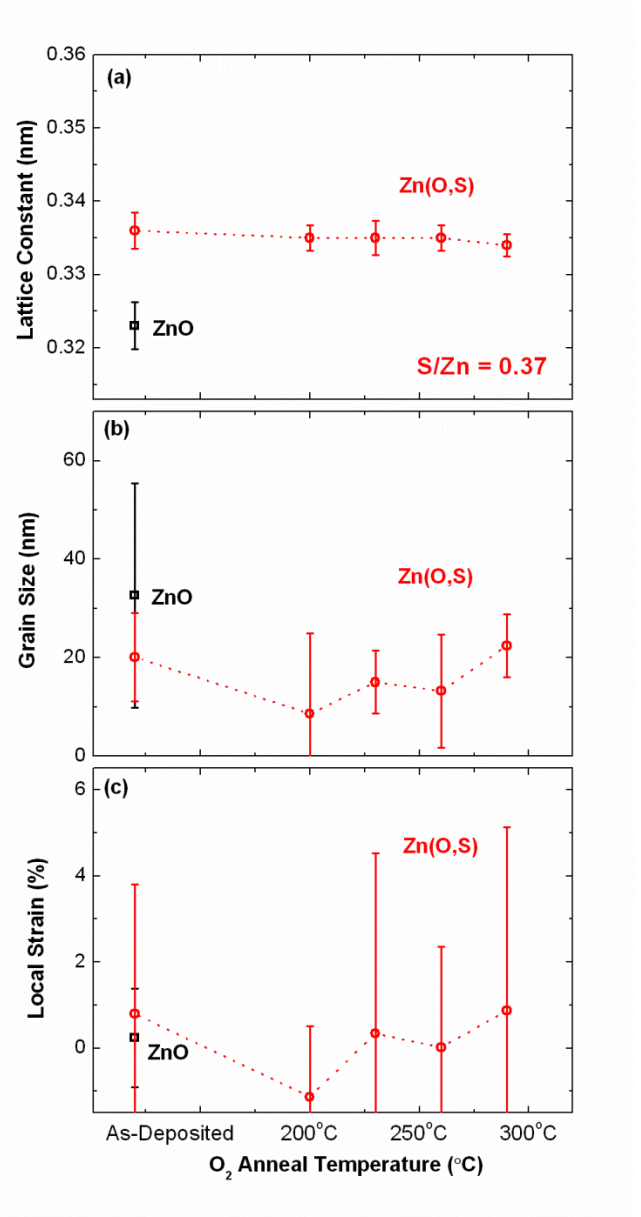

Fig. 5. Plots of (a) lattice constant, (b) grain size, and (c) local strain vs. O_2 annealing temperature for the as-deposited ZnO, as-deposited Zn(O,S) with S/Zn = 0.37, and Zn(O,S) with S/Zn = 0.37, oxygen annealed at different temperatures on quartz substrates.

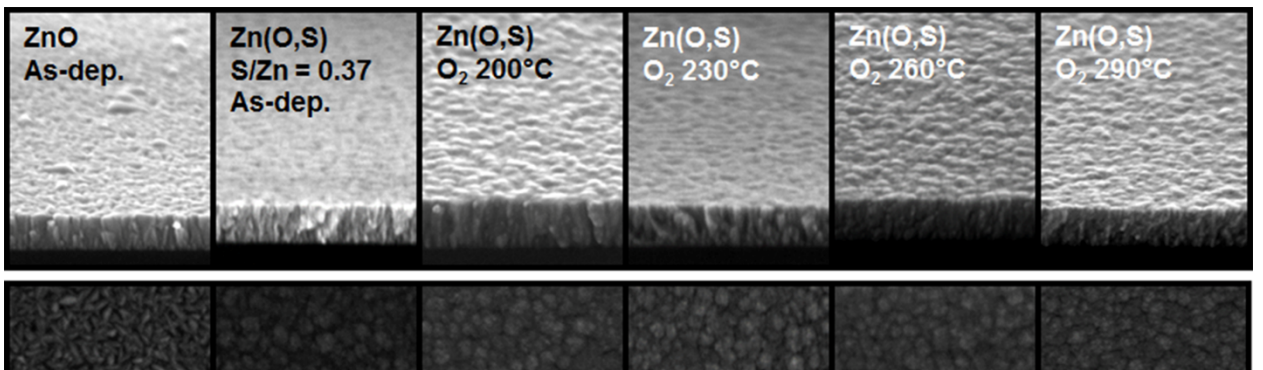

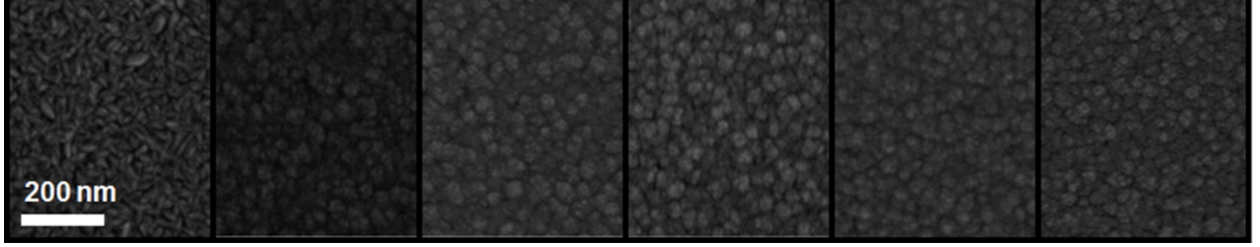

Fig. 6. Cross-sectional and plan-view FESEM images for the as-deposited ZnO, as-deposited Zn(O,S) with S/Zn = 0.37, and Zn(O,S) with S/Zn = 0.37, oxygen annealed at 200°C, 230°C, 260°C, and 290°C.

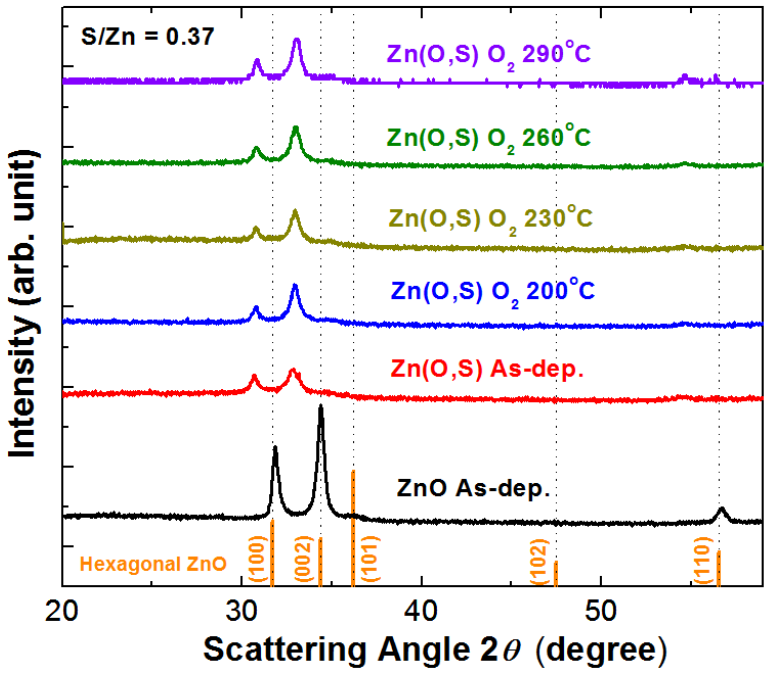

Fig. S1. X-ray diffraction for the as-deposited ZnO, as-deposited Zn(O,S) with S/Zn = 0.37, and Zn(O,S) with S/Zn = 0.37, annealed in O_2 at various temperatures on Si substrates.

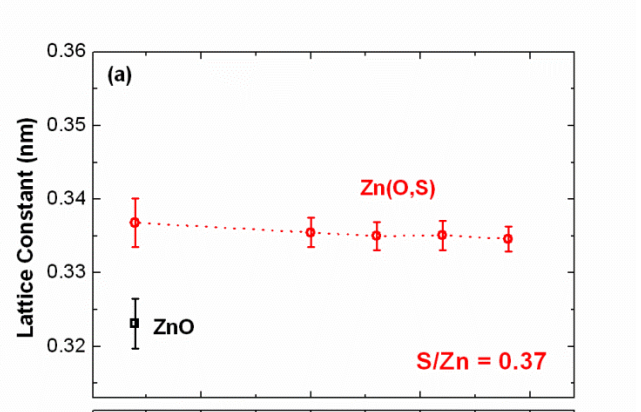

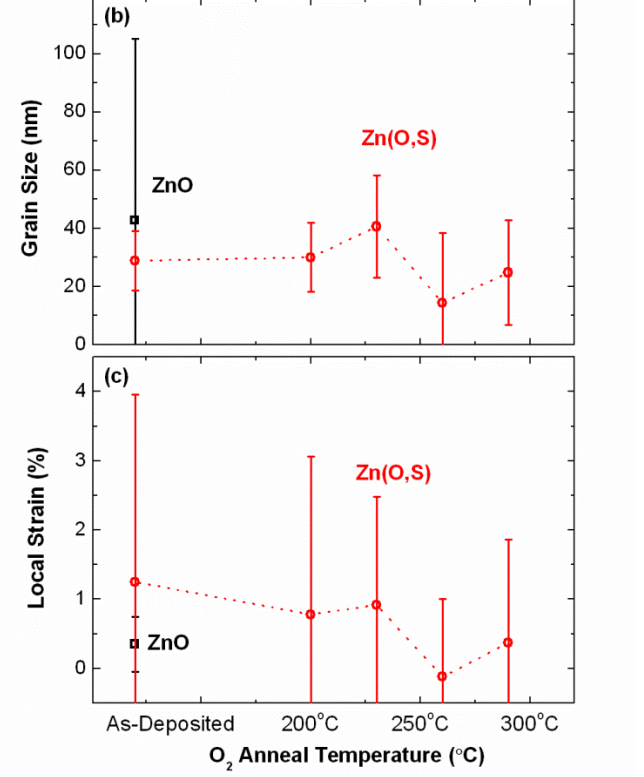

Fig. S2. Plots of (a) lattice constant, (b) grain size, and (c) local strain vs. O_2 annealing temperature for the as-deposited ZnO, as-deposited Zn(O,S) with S/Zn = 0.37, and Zn(O,S) with S/Zn = 0.37, oxygen annealed at different temperatures on Si substrates.